AIP Publishing

This manuscript was accepted by Appl. Phys. Lett. Click here to see the version of record.

Uniformity of cylindrical imploding underwater shockwaves at very small radii

[1]D. Yanuka, [1]A. Rososhek, [2]S.N. Bland and [1]Ya. E. Krasik

[1]Physics Department, Technion, Haifa 32000, Israel

[2]Institute of Shock Physics, Imperial College London, London SW7 2BW, United Kingdom

We compare the convergent shockwaves generated from underwater, cylindrical arrays of copper wire exploded by multiple kilo-ampere current pulses on nanosecond and microsecond-scales. In both cases the pulsed power devices used for the experiments had the same stored energy (~500 J) and the wire mass was adjusted to optimize energy transfer to the shockwave. Laser backlit framing images of the shock front were achieved down to radii of 30 μm. It was found, that even in the case of initial azimuthal non-symmetry, the shock wave self-repairs in the final stages of its motion, leading to a highly uniform implosion. In both these and previous experiments interference fringes have been observed in streak and framing images as the shockwave approached the axis. We have been able to accurately model the origin of the fringes, being due to the propagation of the laser beam diffracting off the uniform converging shock front. The dynamics of the shockwave, and its uniformity at small radii, indicate that even with only 500 J stored energies, this technique should produce pressures above 10^{10} Pa on axis, with temperatures and densities ideal for warm dense matter research.

ACCEPTED MANUSCRIPT

AIP Publishing

This manuscript was accepted by Appl. Phys. Lett. Click here to see the version of record.

The subject of Warm Dense Matter (WDM) has been under intense investigation [1] for several decades due to its importance for many fields of research such as Equations Of State (EOS), conductivity models, astrophysics, geophysics and inertial confinement fusion [2, 3, 4]. There are several methods of obtaining WDM including chemical and nuclear explosions [5], z-pinches [6], high-power lasers [7, 8], light-gas guns [9], and high-energy (GeV range) ion beams [10]. These methods require special safety measures, large and expensive facilities, and stored energies above 10^5 J.

The results of recent studies indicate that WDM with pressures above 100 GPa can be obtained using strong converging Strong Shock Waves (SSW) generated by underwater electrical explosions of either cylindrical or spherical wire arrays [11, 12]. Different methods (damage of different targets, spectroscopy of the obtained water plasma created by the convergence of the SSW) were applied to determine the water parameters in the vicinity of implosion [13, 14, 15]. Also, the SSW's time-of-flight to the axis (cylindrical wire array) or origin (spherical wire array) of implosion leading to intense light emission from compressed and heated water at those locations was used for comparison with the results of one dimensional (1D) and two dimensional (2D) Hydrodynamic (HD) simulations, coupled with the EOS of water and copper [16]. In these simulations, which considered symmetrical SSW convergence, only the energy deposition rate into the wires, calculated using the experimentally obtained resistive voltage and discharge current waveforms, was an input parameter.

In the 1D HD simulations, a symmetrically-propagating SSW is assumed, and in the 2D HD simulations, possible SSW instabilities are not typically taken into account. However, the issue of instabilities, which could lead to a non-uniform azimuthal implosion of the SSW, is of crucial importance for the validity of these simulations, and consequently, for the values of the water

ACCEPTED MANUSCRIPT

AIP Publishing

This manuscript was accepted by Appl. Phys. Lett. Click here to see the version of record.

parameters in the vicinity of implosion. Despite the comprehensive research devoted to converging shock wave instabilities [17, 18, 19], there is no complete understanding regarding the range of applicability and the correctness of the existing models and simulations [20]. Shadowgraph images of converging cylindrical SSWs generated by underwater electrical explosions of wire arrays obtained in experiments carried out in Technion and Imperial College London showed a near circular shape of the SSW's front down to a radius of 100 μm [11, 21, 22].

In this paper, the results of cylindrical SSW convergence below 100 μm radius are described and analyzed. In addition, beam propagation method (BPM) simulations have been applied to study the propagation of a laser beam that is used to backlight framing and streak images of the implosion. The results of these simulations showed interference patterns which almost perfectly fit the inference patterns obtained in these and previous experiments.

The research was carried out using nanosecond and microsecond-scale pulse generators. The nanosecond-scale generator is based on the discharge of a water forming line charged by a Marx generator [23]. This generator, at ±33 kV charging voltage of the Marx generator (stored energy of ~500 J), produces a ~80 ns duration pulse at a 1.5 Ω matched resistive load with voltage and current amplitudes of 120 kV and 50 kA, respectively. The microsecond-scale generator consists of 4 low-inductance, high-voltage capacitors of 0.22 μF each, connected in parallel and a triggered spark gas switch. This generator charged up to 35 kV (stored energy of ~540 J), produces a pulse with a quarter of a period of ~1 μs and an amplitude of 35 kA at a short-circuit load placed instead of the wire array. Both nanosecond and microsecond-scale generators produced at theirs output high voltage pulses with negative polarity. The high-current pulses produced by the nanosecond and microsecond-scale generators were applied to cylindrical wire arrays of 5 mm in diameter, consisting of 20 copper wires, 3 cm in length, and each wire was 23 μm and 50 μm in

ACCEPTED MANUSCRIPT

AIP Publishing

This manuscript was accepted by Appl. Phys. Lett. Click here to see the version of record.

diameter for the nanosecond and microsecond timescales, respectively. Following the action integral [24], this choice of wires should correspond to the wires' explosion at ~0.8 of the maximal current amplitude.

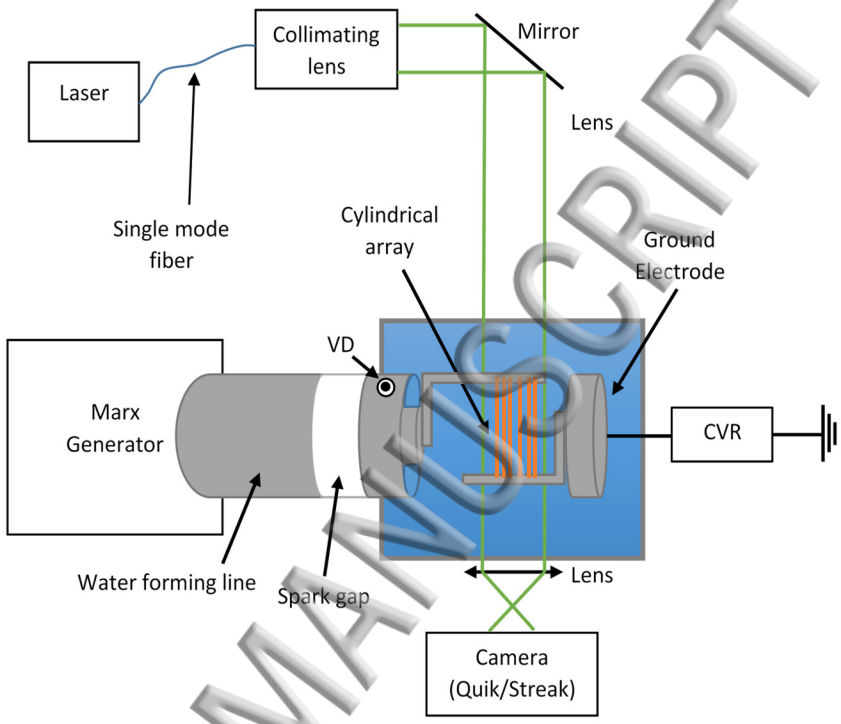

Fig. 1. Experimental setup with nanosecond timescale generator.

The experimental setup is shown in Fig. 1 for the nanosecond timescale (the microsecond timescale setup is identical except for the generator used). A single mode 532 nm, 2.5 W, continuous wave laser (by Roithner Lasertechnik GmbH) was used for the backlighting of the converging SSWs. The laser was coupled to a single mode fiber to spatially filter the beam, removing/reducing any speckle effect in subsequent images. The output from the fiber was collimated to produce a ~3 mm radius beam that was directed through a fused silica window into the water-filled stainless steel chamber coaxial with the wire array (see Fig. 1). An imaging lens was placed outside of the chamber to image the SSW's front to either a XXRapidFrame framing

ACCEPTED MANUSCRIPT

AIP Publishing

This manuscript was accepted by Appl. Phys. Lett. Click here to see the version of record.

camera (Stanford Computer Optics, Germany) allowing four time-independent frames with a duration above 1 ns, or a SC-10 streak camera (Optronis GmbH, Germany). The discharge current I through the wire was measured using a current view resistor, and the voltage drop φ across the exploding wire was measured using a capacitive voltage divider.

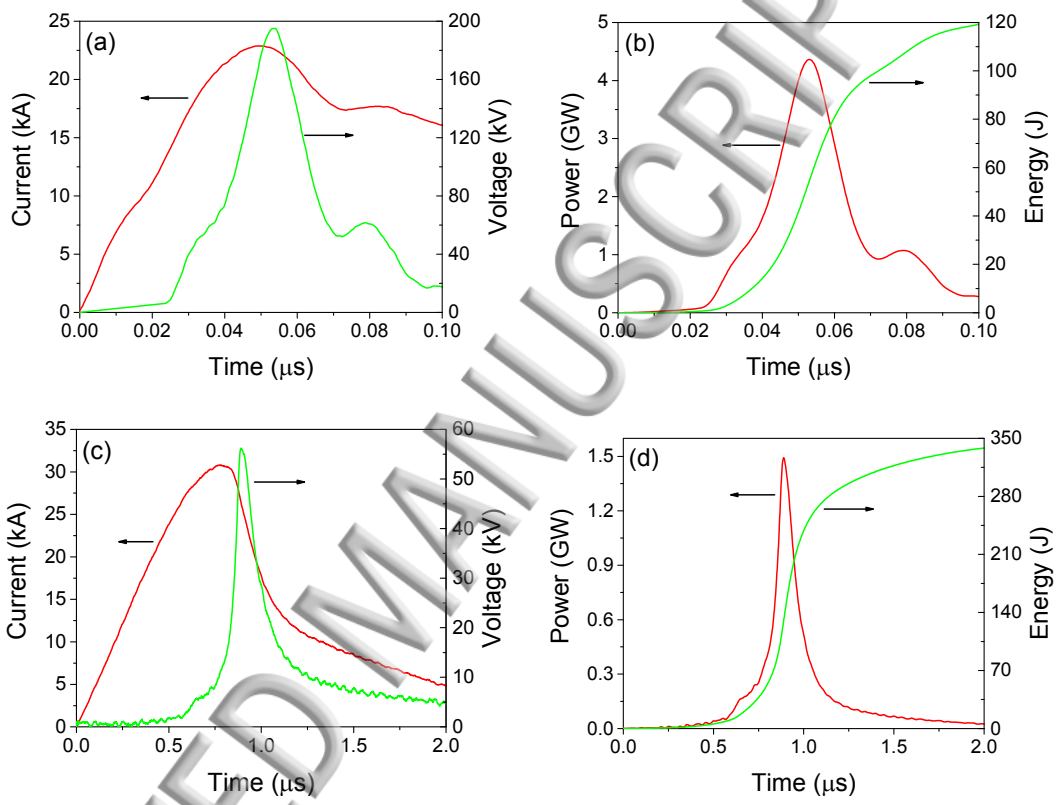

Fig. 2. Waveforms of the measured current and resistive voltage for (a) nanosecond and (c) microsecond-scale wire array explosions. Calculated power and energy for (b) nanosecond and (d) microsecond-scale wire array explosions.

Typical current, resistive voltage $\varphi_r = \varphi - LdI/dt$ (L is the load's inductance), power, and deposited energy waveforms are shown in Fig. 2 for the nanosecond and microsecond-scale explosions. The deposited power and energy were calculated using the experimentally obtained current and voltage waveforms. One can see that the selection of the wires' parameters allowed us to obtain almost critically damped discharges where most of the stored energy was deposited into

ACCEPTED MANUSCRIPT

AIP Publishing

This manuscript was accepted by Appl. Phys. Lett. Click here to see the version of record.

ing wires during ~100 ns and ~1200 ns in the nanosecond and microsecond-scale explosions, respectively. The maximal current densities realized in the exploding wires were below 6000 MA/cm^2 and 1600 MA/cm^2 for the nanosecond and microsecond-scale explosions, respectively.

For each timescale, shadowgraph images of the SSW's front were obtained at low magnification (~6 mm in diameter) with the exploding wires included in the frame, and at high magnification (≤1 mm in diameter) to obtain only the final stages of the SSW's convergence.

Low magnification framing images from both nanosecond and microsecond-scale experiments showed that when the imploding shock front was formed from the overlapping explosions of adjacent wires, it was often not azimuthally symmetric. This can be related to a technical problem of placing the wires uniformly around on a small diameter (with an equal distance of 0.75 mm between them). An example of such initial azimuthal deformation of the shock front is shown in Fig. 3(a) where three overlapping frames obtained by the XXRapidFrame camera are shown for a microsecond timescale explosion. Typical overlapping images of a nearly circular azimuthal symmetry are shown for comparison in Fig. 3 (b) and (c).

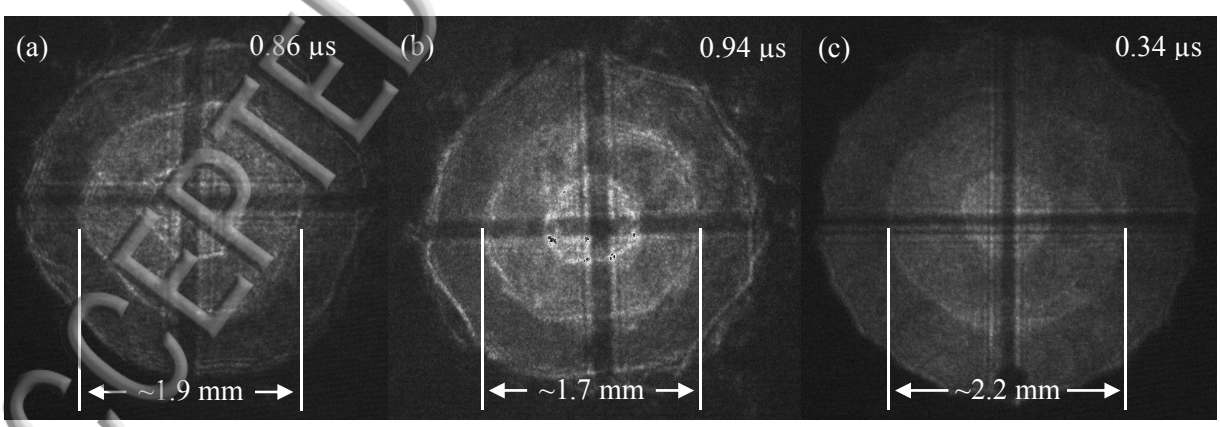

Fig. 3. Three overlapping shadowgraph images of the SSW front with (a) azimuthal non-uniformity; (b) and (c) nearly circular symmetry. (a) and (b) are for the microsecond timescale, and (c) for the nanosecond timescale. The times are with respect to the beginning of the discharge current and the time between each frame is 300 ns. Each frame duration is 2 ns. The cross in the images is because of wires placed at the front and back sides of the array for optical alignment.

ACCEPTED MANUSCRIPT

AIP Publishing

This manuscript was accepted by Appl. Phys. Lett. Click here to see the version of record.

Experiments at high magnification were complicated by the need for extremely high accuracy in aligning the laser with the axis of the array, i.e. better than 1^0 alignment is needed in order to obtain images at radii below 0.1 mm, otherwise the perfectly cylindrical implosions are obscured and appear to be elliptical. With improvements in the alignment technique, it was found that even shockwaves that were initially highly asymmetric tended to repair themselves as they imploded towards the axis. Typical shadowgraph images of the converging SSW for nanosecond and microsecond-scale are shown in Fig. 4. Here four separate shadowgraph images are presented, obtained by the XXRapidFrame camera, for better accuracy of the SSW imaging at higher SSW velocity. One can see clearly the self-repairing nature of the SSW's evolution especially at the final stage of implosion. In the first frame of the nanosecond timescale image (Fig. 4a), the radius of the SSW front is ~190 μm and the front is rather azimuthally non-uniform. But by the third frame (Fig. 4c), obtained with a delay of 50 ns with respect to the first frame, there is almost circular front. Finally, the fourth frame (Fig. 4d), obtained with 20 ns with respect to the third frame, showed no detectable instabilities at a radius of ~30 μm. Similar self-repair of the converging shock front was obtained for the microsecond timescale experiments (Fig 4(e-h)), where the shock wave's radius is ~275 μm in the first frame (Fig. 4e) and reaches a radius of ~35 μm by the fourth frame (Fig. 4h) obtained with time delay of 150 ns with respect to the first frame. Here let us note that there were difficulties related to obtaining shadowgraph images of the SSW at radii smaller than 30 μm. The first difficulty was in the triggering of the framing camera when the SSW arrived to a radius below 30 μm, because it takes only several nanoseconds for the SSW to arrive to the origin from that position. Also, taking shadowgraph images at radii smaller than 30 μm becomes challenging because the shockwave begins to radiate (due to high temperature and

ACCEPTED MANUSCRIPT

AIP Publishing

This manuscript was accepted by Appl. Phys. Lett. Click here to see the version of record.

density of water behind the shock front) and generates a plasma layer with thickness of several microns in front of the shockwave, thus smearing its front.

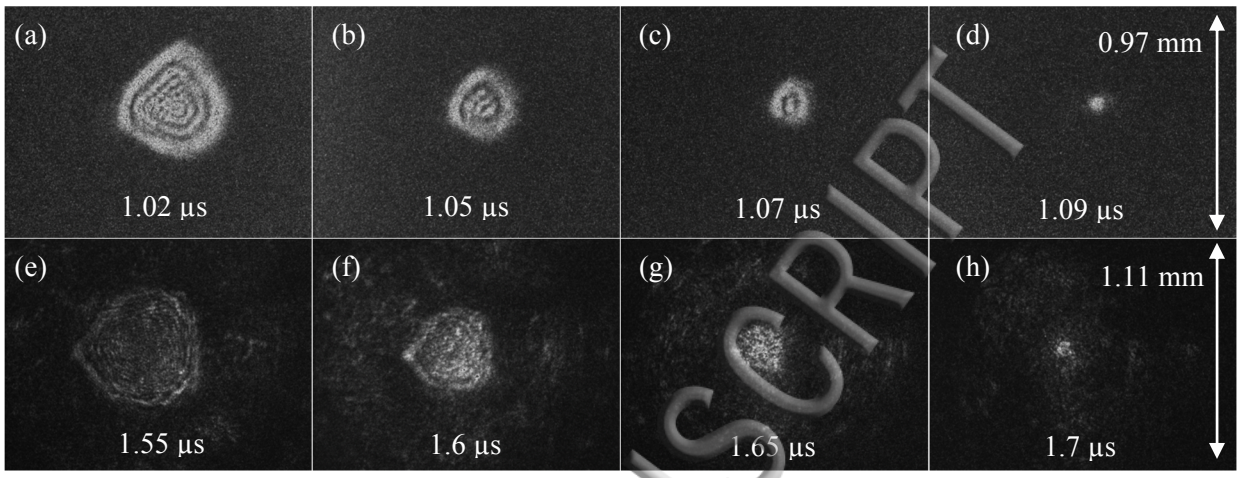

Fig. 4. Shadowgraph images of the SSWs obtained with large magnification at different times for the (a-d) nanosecond and (e-h) microsecond timescales wire array electrical explosions. Each frame time duration is of 2 ns. The times are relative to the beginning of the discharge current.

In these and previous experiments, interference fringes are clearly visible in both high magnification framing images and laser backlit streak photographs taken across the diameter of the array. To explain the fringes, a 2D fast Fourier transform-based BPM simulation [25] was carried out. In these simulations the laser beam is considered as a wave propagating inside the cylinder which models the shock front. The wave propagation is governed by the Helmholtz equation in the paraxial approximation, i.e. the amplitude of the wave is varying slowly outwards from the axis (along the x-axis in our case), and rapidly in the direction of propagation (along the z axis in our case). The boundary conditions are the values of the refractive index $n(x, z)$ and the initial condition is the amplitude of the wave. Because the boundary of the SSW is highly reflective, the refractive index was set to be two orders of magnitude larger at the location of the SSW and outwards than the refractive index of water inside the cylinder, which was set to 1.32. These simulations do not account for the acceleration of the SSW during its convergence towards

ACCEPTED MANUSCRIPT

AIP Publishing

This manuscript was accepted by Appl. Phys. Lett. Click here to see the version of record.

ing axis, i.e. the decrease of the cylinder's radius versus time was considered linear, which is applicable to the majority of the implosion.

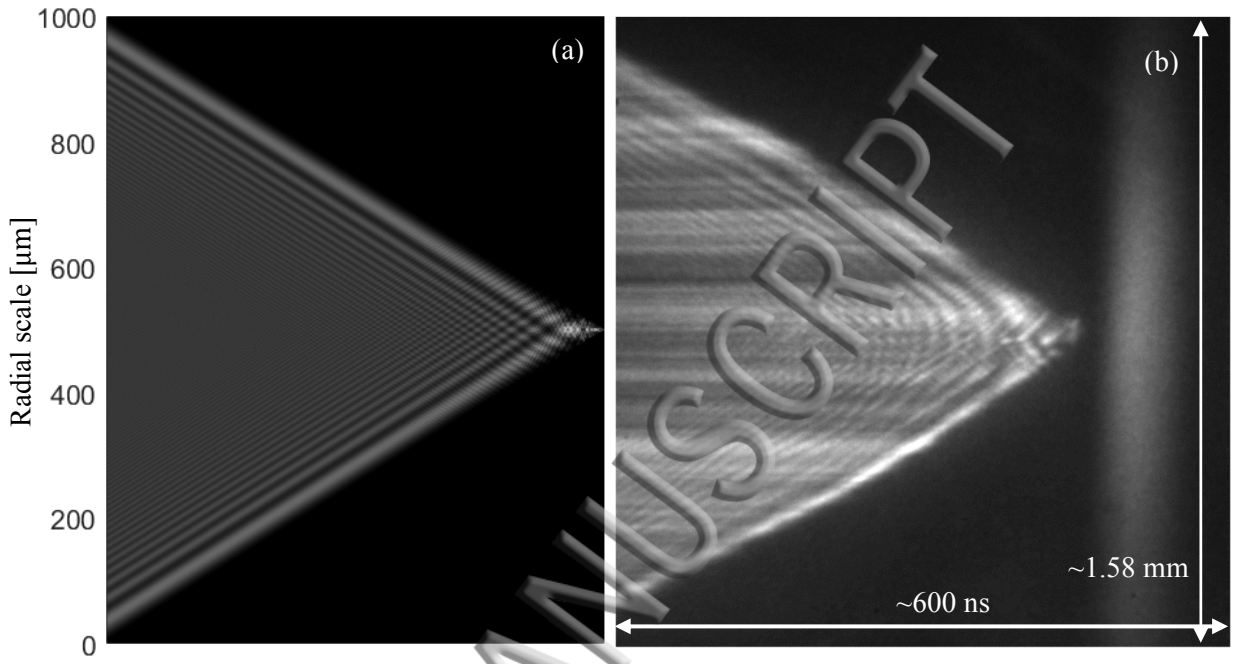

Fig. 5. Time dependent light intensity in the middle of the cylinder obtained by (a) BPM simulation and (b) streak shadowgraph imaging of the converging SSW.

The plot in Fig. 5a represents the results of BMP simulations of the light intensity, which one can obtain in the middle of the cylinder for different SSW radii, i.e. at different times of the SSW's convergence. Experiments with the SC-10 streak camera (the width of the input slit is of 0.1 mm and the focus of the camera was at the middle of the array) were carried out to obtain a shadowgraph streak image of the converging SSW and compare to the simulation results. One can see a good agreement between the fringes obtained in the experiments and simulations. The slopes of the experimental and simulated fringes are almost linear and coincide during the first ~300 ns and correspond to ~1.75×10^5 cm/s of SSW velocity. Later, the slop of experimental fringes increases due to the SSW's acceleration towards the axis during the final stage of implosion. The coincidence between the simulated and experimentally obtained fringes during around 300 ns of

ACCEPTED MANUSCRIPT

AIP Publishing

This manuscript was accepted by Appl. Phys. Lett. Click here to see the version of record.

the shockwave's propagation indicates on azimuthal and longitudinal uniformity of the converging shockwave. In addition, in Fig. 5(b) one can see a strong light emission which indicates on high water temperature and density in the vicinity of implosion. The duration of this light emission is ~100 ns and the time difference between the end of the resolvable streak image of the converging SSW front and the beginning of this light emission is less than 15 ns. This time delay can be related to a small misaligning the slit of the streak camera and the axis of the converging SSW. The SSW's velocity at radii below 50 μm, estimated by the streak image of the SSW, is larger than 3×10^5 cm/s. This allows one to estimate the minimal radius where the SSW was obtained at ~45 μm. Let us note that in order to obtain the SSW's convergence at smaller radii, the alignment of the optical system should be better than 1.5×10^{-3} degree. Thus, the BPM simulations and experimentally obtained streak shadowgraph images confirm the uniformity of the SSW convergence up to a compression factor of ~60.

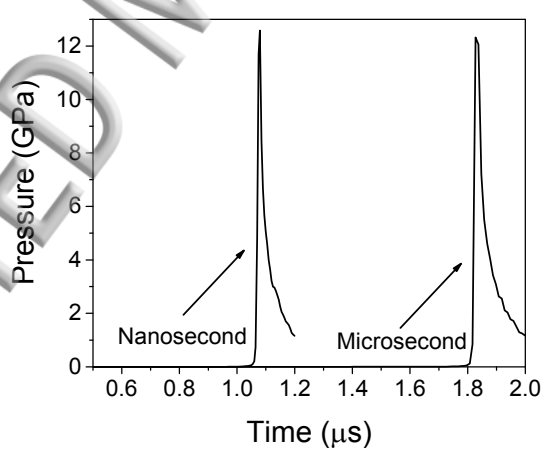

Fig. 6. Pressure at radius 30 μm for the nanosecond and microsecond timescales.

The present experimental results show an implosion down to at least 60 μm in diameter. The pressure of water at that location was calculated using a 2D HD simulation coupled with EOSs of water and copper. These simulations, based on the cell-centered finite volume method and three

ACCEPTED MANUSCRIPT

AIP Publishing

This manuscript was accepted by Appl. Phys. Lett. Click here to see the version of record.

conservation laws (mass, momentum, and energy) are described in detail by Kozlov *et al*. [16]. The results of these simulations are shown in Fig. 6. One can see that in both nanosecond and microsecond-scale array explosions at $r \leq 30\ \mu m$, one should obtain pressure above 1.2×10^{10} Pa. Considering self-similarity [26] of the SSW implosion and assuming azimuthal uniformity of the SSW during the last 15 ns of convergence, one can expect to obtain pressure larger than 4×10^{10} Pa at $r \leq 5\ \mu m$.

In summary, we carried out research on the convergence of shockwaves generated by both nanosecond and microsecond-scale underwater electrical explosions of cylindrical copper wire arrays. Experiments demonstrated that even in the case of an initially azimuthally asymmetric implosion, the SSW self-repairs as it approaches the axis. The interference fringes observed in both framing and streak images of the implosion were found to agree with the results of BPM simulations. The framing shadowgraph images showed the absence of detectable instabilities of the SSW front down to radii of 30 μm. Thus, this research indicated that using a pulsed power generator with stored energy of only ~500 J, one can produce pressures above 10^{10} Pa in the vicinity of the implosion of the SSW. Such a compact and mobile setup can be easily adjusted for the diagnostics of warm dense matter density distribution using either synchrotron radiation or x-ray fluxes produced by powerful lasers.

Acknowledgments

The authors are grateful to M. Nitishinski and S. Efimov for fruitful discussions and to S. Gleizer for technical assistance.

ACCEPTED MANUSCRIPT

AIP Publishing

This manuscript was accepted by Appl. Phys. Lett. Click here to see the version of record.

References

[1] V. E. Fortov, Extreme states of matter, Berlin Heidelberg: Springer-Verlag, 2011.

[2] P. Renaudin, C. Blancard, J. Clerouin, G. Faussurier, P. Noiret and V. Recoules, "Aluminum Equation-of-State Data in the Warm Dense Matter Regime," *Phys. Rev. Lett.,* vol. 91, p. 075002, 2003.

[3] G. W. Collins, L. B. Da Silva, P. Celliers, D. M. Gold, M. E. Foord, R. J. Wallace, A. Ng, S. V. Weber, K. S. Budil and R. Cauble, "Measurements of the Equation of State of Deuterium at the Fluid Insulator-Metal Transition," *Science,* vol. 281, p. 1178, 1998.

[4] G. Huser, M. Koenig, A. Benuzzi-Mounaix, E. Henry, T. Vinci, B. Faral, M. Tomasini, B. Telaro and D. Batani, "Temperature and melting of laser-shocked iron releasing," *Phys. Plasmas,* vol. 12, p. 060701, 2005.

[5] E. N. Avrorin, B. K. Vodolaga, V. A. Simonenko and V. E. Fortov, "Intense shock waves and extreme states of matter," *Physics-Uspekhi,* vol. 36, p. 337, 1993.

[6] M. C. Jones, D. J. Ampleford, M. E. Cuneo, R. Hohlfelder, C. A. Jennings, D. W. Johnson, B. Jones, M. R. Lopez, J. MacArthur, J. A. Mills, T. Preston, G. A. Rochau, M. Savage, D. Spencer, D. B. Sinars and J. L. Porter, "X-ray power and yield measurements at the refurbished Z machine," *Rev. Sci. Instrum.,* vol. 85, p. 083501, 2014.

[7] B. A. Hammel and National Ignition Campaign Team, "The NIF Ignition Program: progress and planning," *Plasma Phys. Control. Fusion,* vol. 48, p. B497, 2006.

ACCEPTED MANUSCRIPT

AIP Publishing

This manuscript was accepted by Appl. Phys. Lett. Click here to see the version of record.

[8] T. R. Boehly, E. Vianello, J. E. Miller, R. S. Craxton, T. J. Collins, V. N. Goncharov, I. V. Igumenshchev, D. D. Meyerhofer, D. G. Hicks, P. M. Celliers and G. W. Collins, "Shock-timing experiments using double-pulse laser irradiation," *Phys. Plasmas,* vol. 13, p. 056303, 2006.

[9] A. H. Jones, W. M. Isbell and C. J. Maiden, "Measurement of the Very-High-Pressure Properties of Materials using a Light-Gas Gun," *J. Appl. Phys.,* vol. 37, p. 3493, 1966.

[10] C. L. Morris, N. S. King, K. Kwiatkowski, F. G. Mariam, F. E. Merrill and A. Saunders, "Charged particle radiography," *Rep. Prog. Phys.,* vol. 76, p. 046301, 2013.

[11] S. N. Bland, Y. E. Krasik, D. Yanuka, R. Gardner, J. MacDonald, A. Virozub, S. Efimov, S. Gleizer and N. Chaturvedi, "Generation of highly symmetric, cylindrically convergent shockwaves in water," *Phys. Plasmas ,* vol. 24, p. 082702, 2017.

[12] D. Yanuka, A. Rososhek, S. Efimov, M. Nitishinskiy and Y. E. Krasik, "Time-resolved spectroscopy of light emission from plasma generated by a converging strong shock wave in water," *Appl. Phys. Lett.,* vol. 109, p. 244101, 2016.

[13] O. Antonov, S. Efimov, V. T. Gurovich, D. Yanuka, D. Shafer and Y. E. Krasik, "Diagnostics of a converging strong shock wave generated by underwater explosion of spherical wire array," *J. Appl. Phys.,* vol. 115, p. 223303, 2014.

[14] O. Antonov, S. Efimov, V. T. Gurovich, V. Bernshtam and Y. E. Krasik, "Spectroscopy of a plasma formed in the vicinity of implosion of the shock wave generated by underwater electrical explosion of spherical wire array," *Phys. Plasmas,* vol. 22, p. 053507, 2015.

ACCEPTED MANUSCRIPT

AIP Publishing

This manuscript was accepted by Appl. Phys. Lett. Click here to see the version of record.

[15] M. Nitishinskiy, S. Efimov, O. Antonov, D. Yanuka, V. T. Gurovich, V. Bernshtam, V. Fisher and Y. E. Krasik, "Converging shock wave focusing and interaction with a target," *Phys. Plasmas,* vol. 23, p. 042705, 2016.

[16] M. Kozlov, V. T. Gurovich and Y. E. Krasik, "Stability of imploding shocks generated by underwater electrical explosion of cylindrical wire array," *Phys. Plasmas,* vol. 20, p. 112701, 2013.

[17] J. H. Gardner, D. L. Book and I. B. Bernstein, "Stability of imploding shocks in the CCW approximation," *J. Fluid Mech.,* vol. 114, p. 41, 1982.

[18] V. Eliasson, M. Kjellander and N. Apazidis, "Regular versus Mach reflection for converging polygonal shocks," *Shock Waves,* vol. 17, p. 43, 2007.

[19] S. E. Bodner, "Rayleigh-Taylor Instability and Laser-Pellet Fusion," *Phys. Rev. Lett.,* vol. 33, p. 761, 1974.

[20] G. B. Whitham, Linear and Nonlinear Waves, New York: Wiley-Interscience, 1999.

[21] L. Gilburd, S. Efimov, A. Fedotov Gefen, V. T. Gurovich, G. Bazalitski, O. Antonov and Y. E. Krasik, "Modified wire array underwater electrical explosion," *Laser and Particle Beams,* p. 1, 2012.

[22] A. Fedotov-Gefen, S. Efimov, L. Gilburd, G. Bazalitski, V. T. Gurovich and Y. E. Krasik, "Generation of a 400 GPa pressure in water using converging strong shock waves," *Phys. Plasmas,* vol. 18, p. 062701, 2011.

ACCEPTED MANUSCRIPT

AIP Publishing

This manuscript was accepted by Appl. Phys. Lett. Click here to see the version of record.

[23] A. Grinenko, Y. E. Krasik, S. Efimov, A. Fedotov, V. T. Gurovich and V. I. Oreshkin, "Nanosecond time scale, high power electrical wire explosion in water," *Phys. Plasmas,* vol. 13, p. 042701, 2006.

[24] S. A. Chikovsky, V. I. Oreshkin, G. A. Mesyats, N. A. Ratakhin, I. M. Datsko and B. A. Kablambaev, "Electrical explosion of metals in fast-rising megagauss magnetic fields," *Phys. Plasmas,* vol. 16, p. 042701, 2009.

[25] K. Okamoto, Fundamentals of Optical Waveguides, Academic Press, 2006.

[26] A. Grinenko, V. T. Gurovich and Y. E. Krasik, "Implosion in water medium and its possible application for the inertial confinement fusion target ignition," *Phys. Plasmas,* vol. 14, p. 012701, 2007.

ACCEPTED MANUSCRIPT

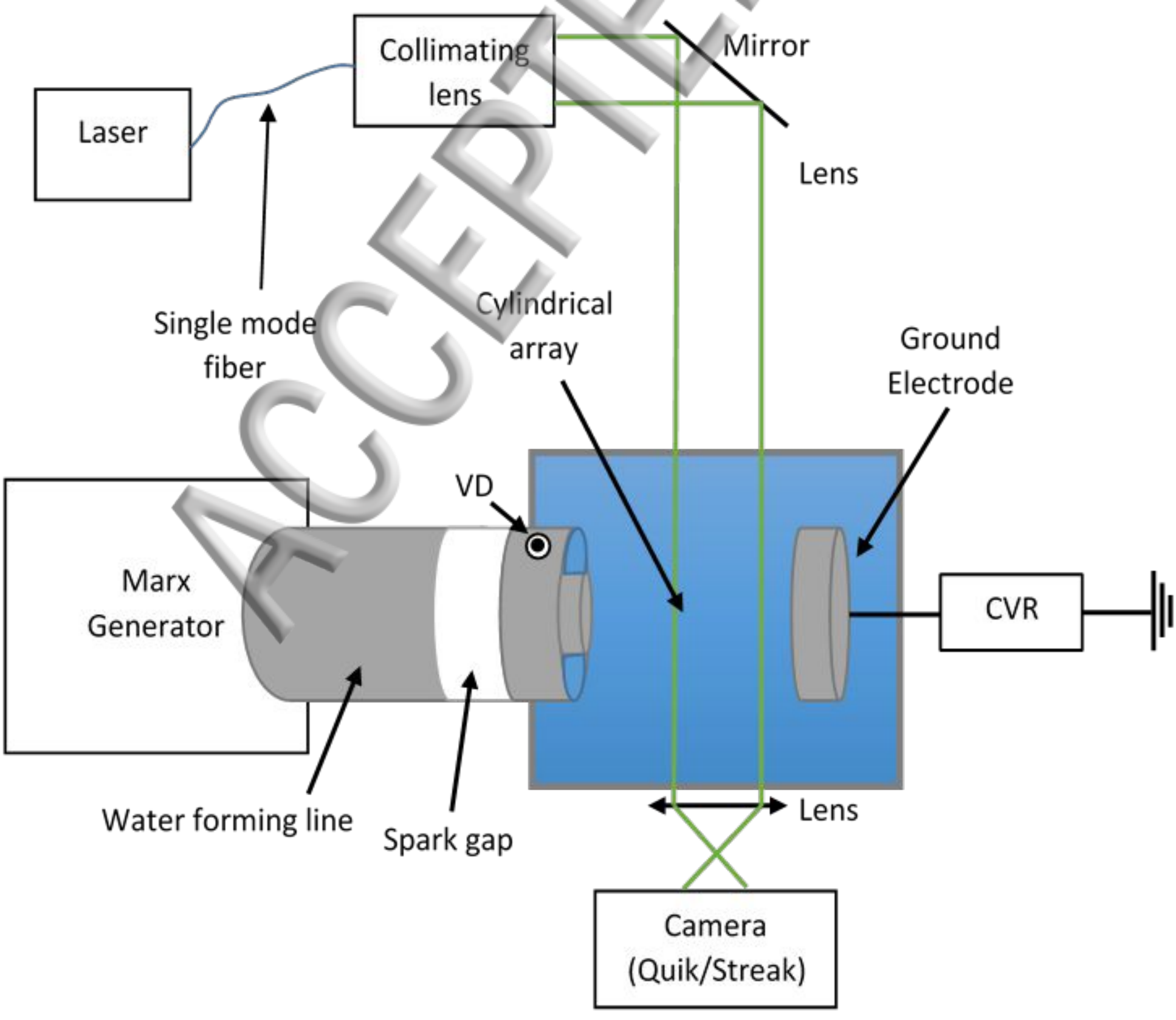
Collimating lens
Mirror
Laser
Lens
Single mode fiber
Cylindrical array
Ground Electrode
VD
Marx Generator
CVR
Water forming line
Spark gap
Lens
Camera (Quik/Streak)
ACCEPTED

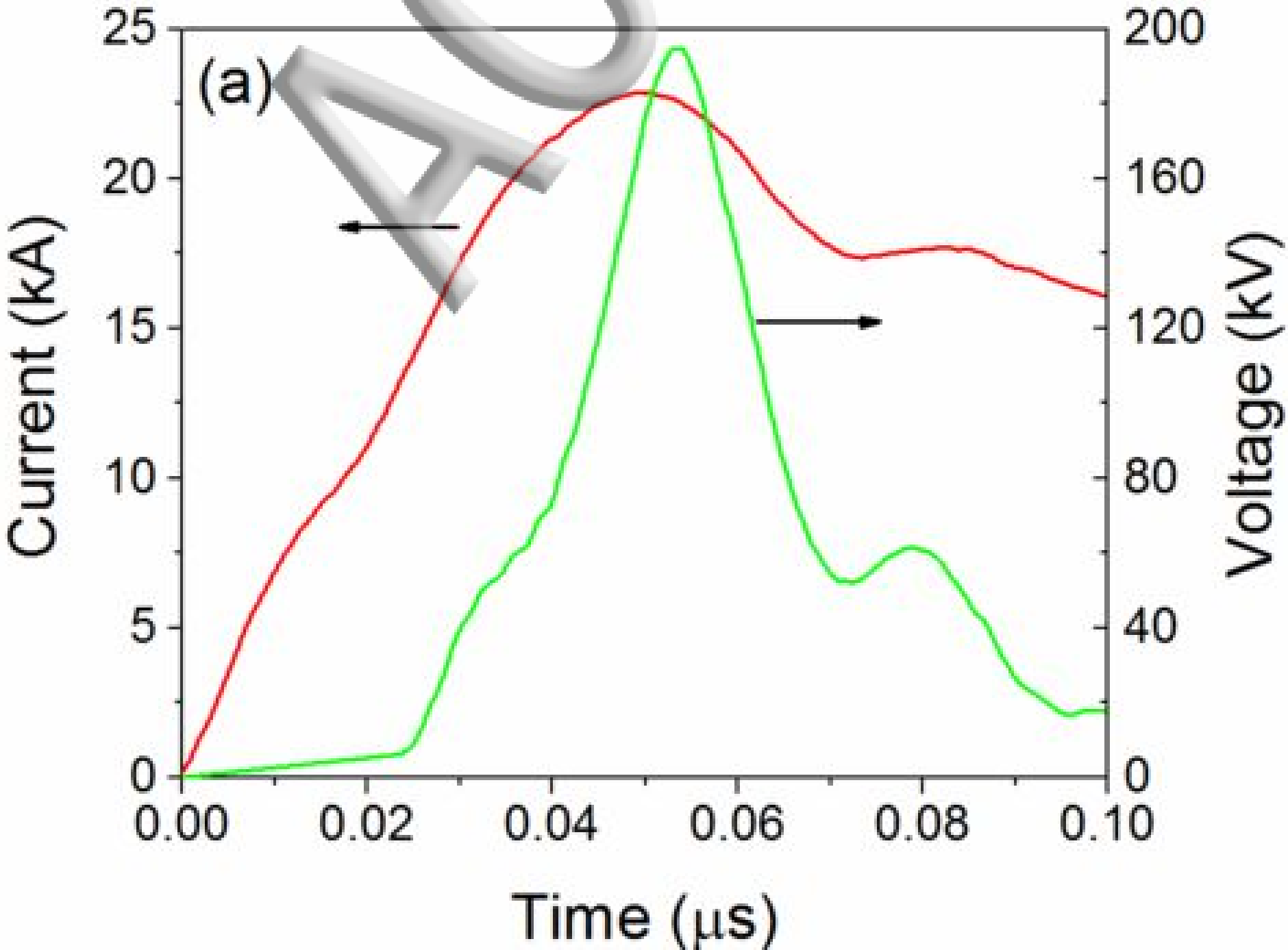
(a)
Current (kA)
Voltage (kV)
Time (μs)
0
5
10
15
20
25
0
40
80
120
160
200
0.00
0.02
0.04
0.06
0.08
0.10

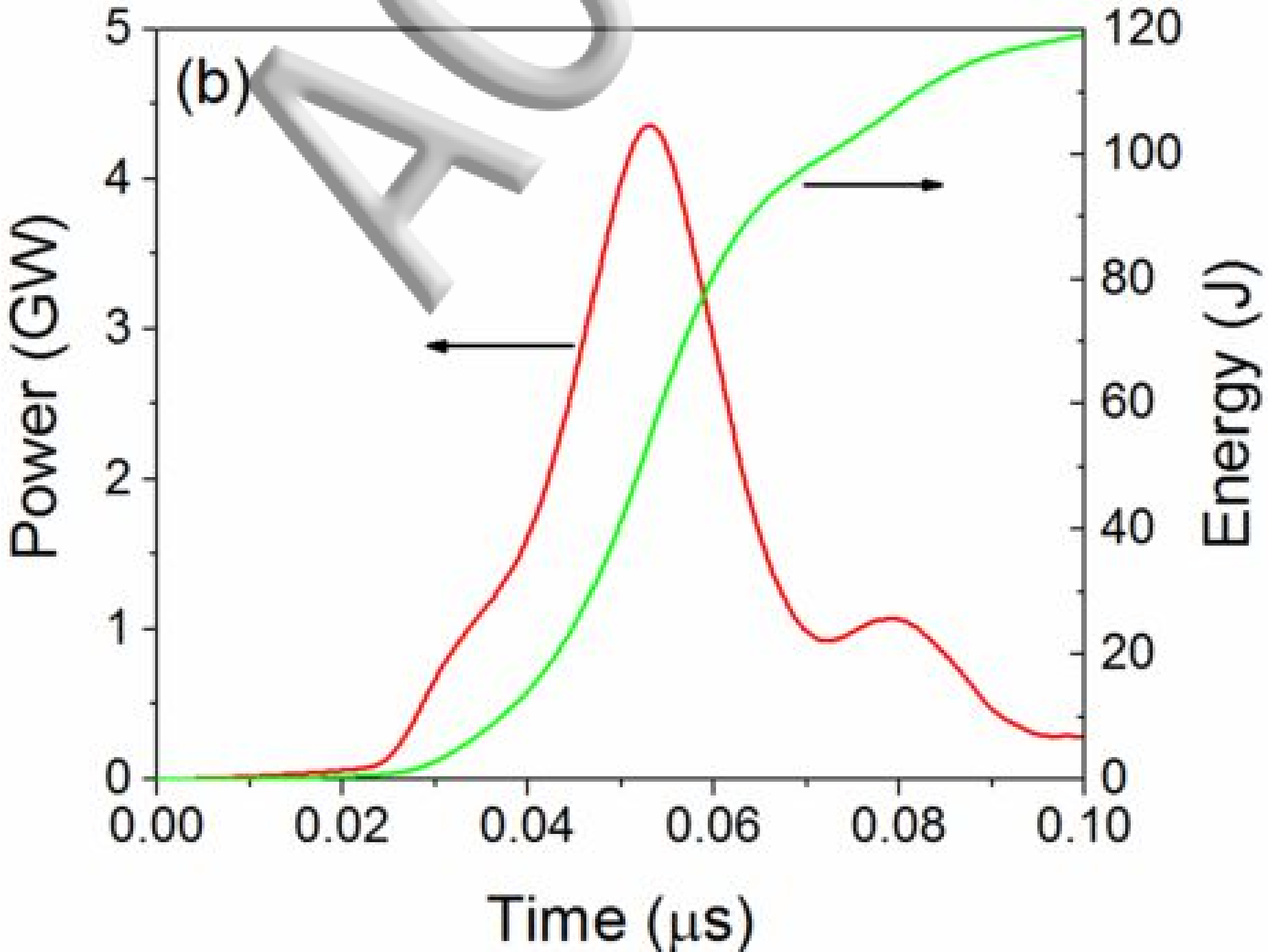
(b)
Power (GW)
Energy (J)
Time (μs)
0
1
2
3
4
5
0
20
40
60
80
100
120
0.00
0.02
0.04
0.06
0.08
0.10

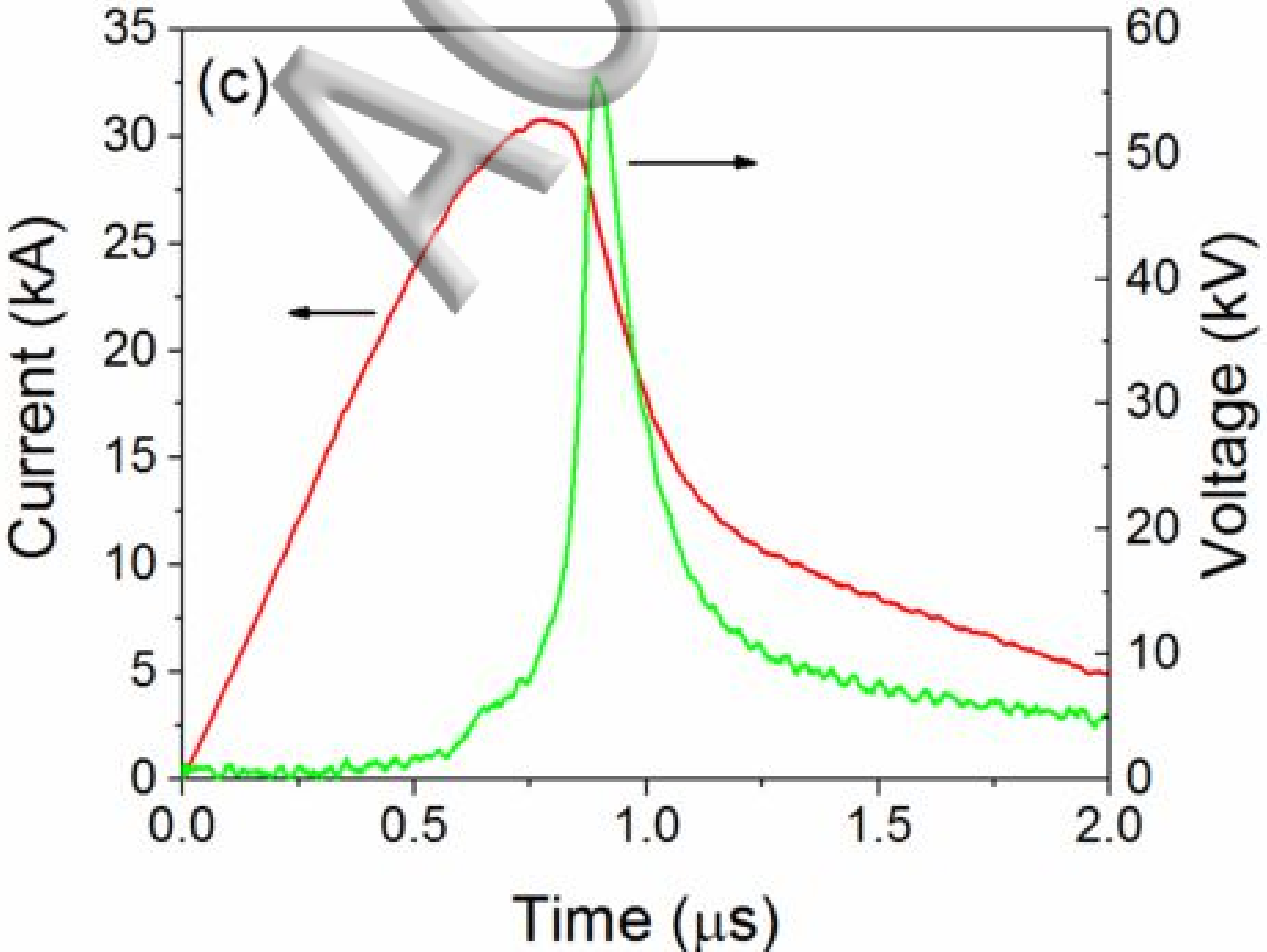
(c)
Current (kA)
Voltage (kV)
Time (μs)
0
5
10
15
20
25
30
35
0
10
20
30
40
50
60
0.0
0.5
1.0
1.5
2.0

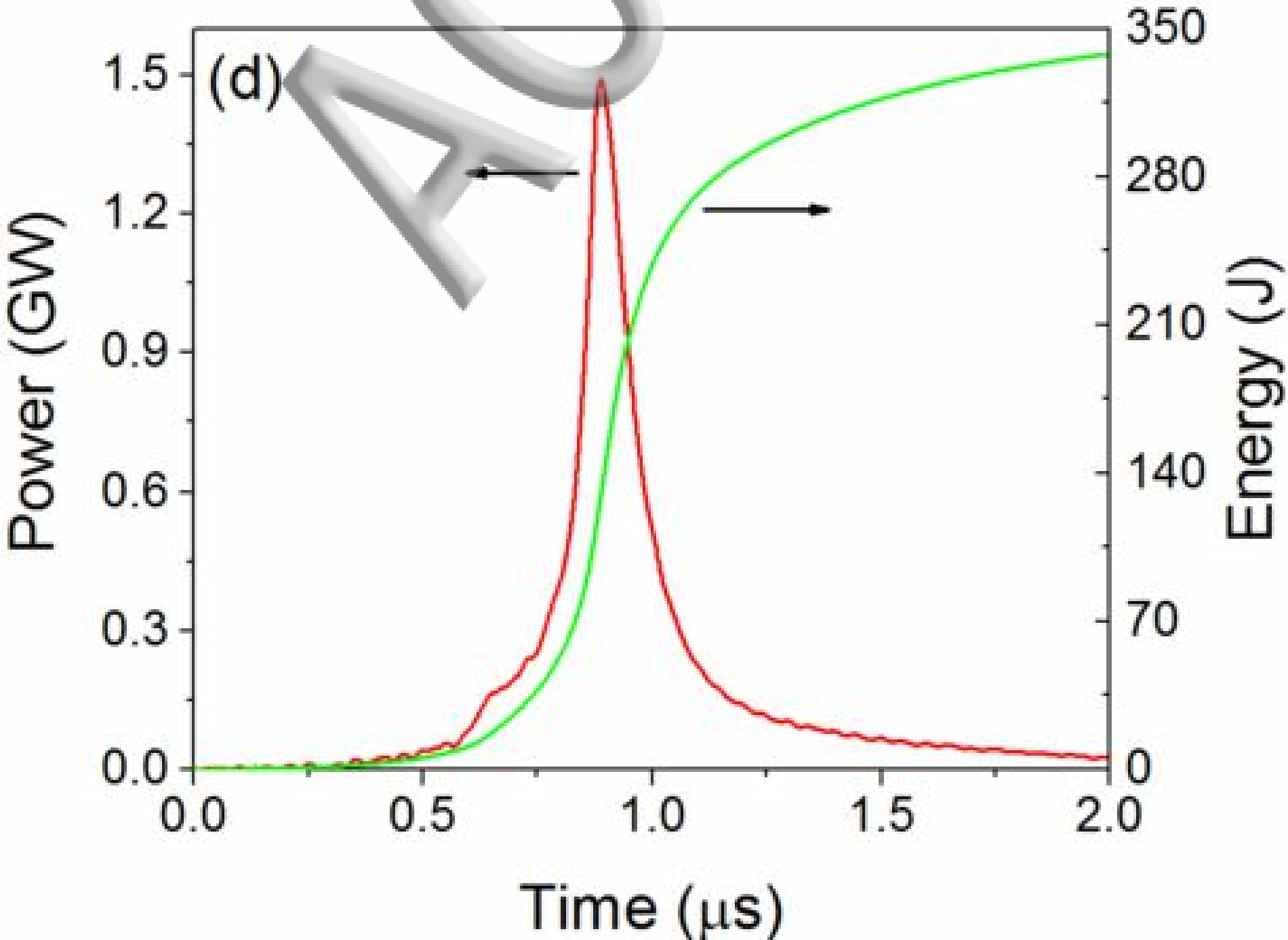
(d)
Power (GW)
Energy (J)
Time (μs)
0.0
0.3
0.6
0.9
1.2
1.5
0
70
140
210
280
350
0.0
0.5
1.0
1.5
2.0

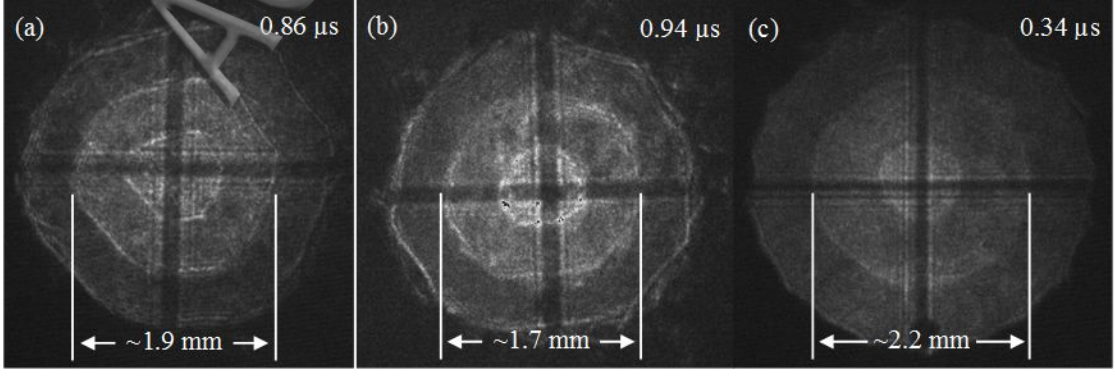
(a)
0.86 µs
~1.9 mm
(b)
0.94 µs
~1.7 mm
(c)
0.34 µs
~2.2 mm

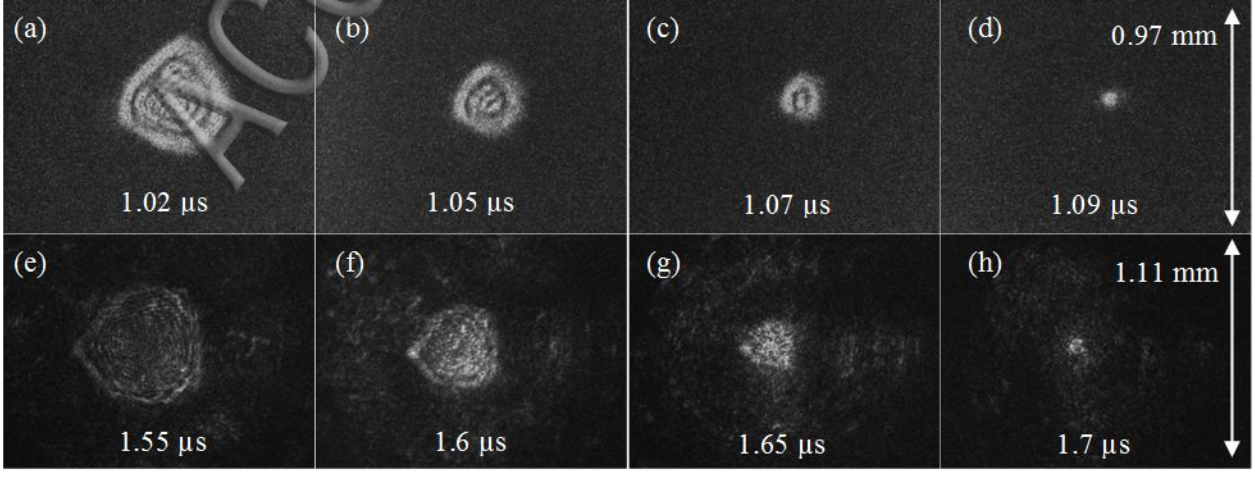
(a)
1.02 µs
(b)
1.05 µs
(c)
1.07 µs
(d)
0.97 mm
1.09 µs
(e)
1.55 µs
(f)
1.6 µs
(g)
1.65 µs
(h)
1.11 mm
1.7 µs

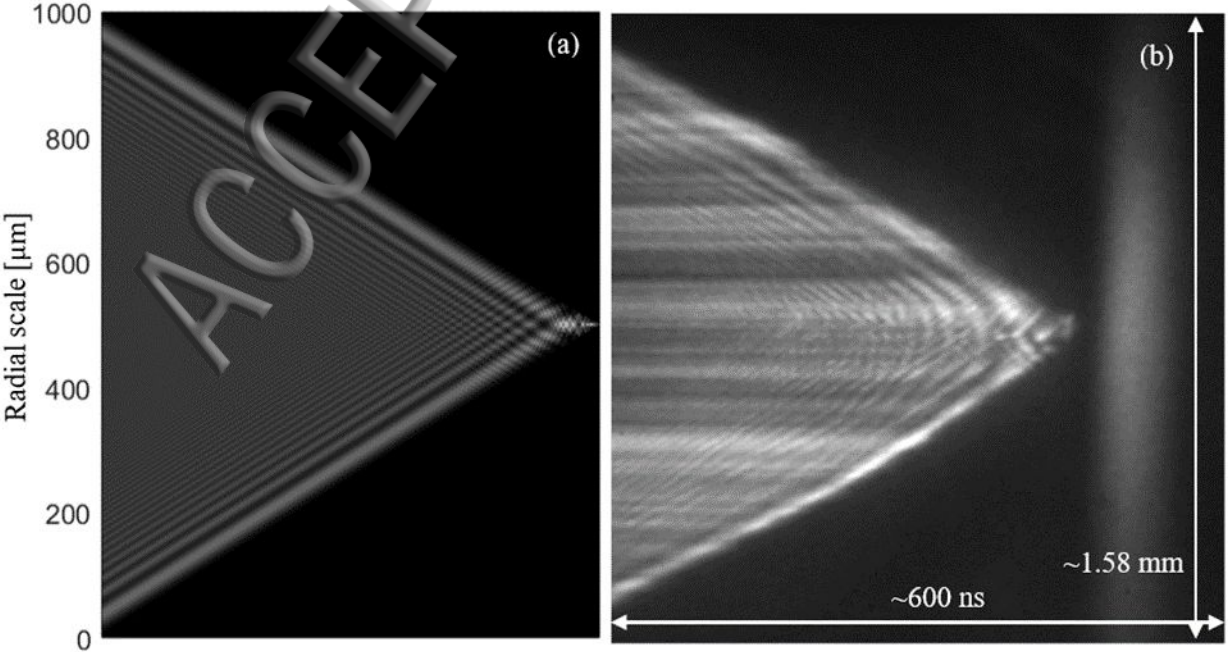

ACCEPT

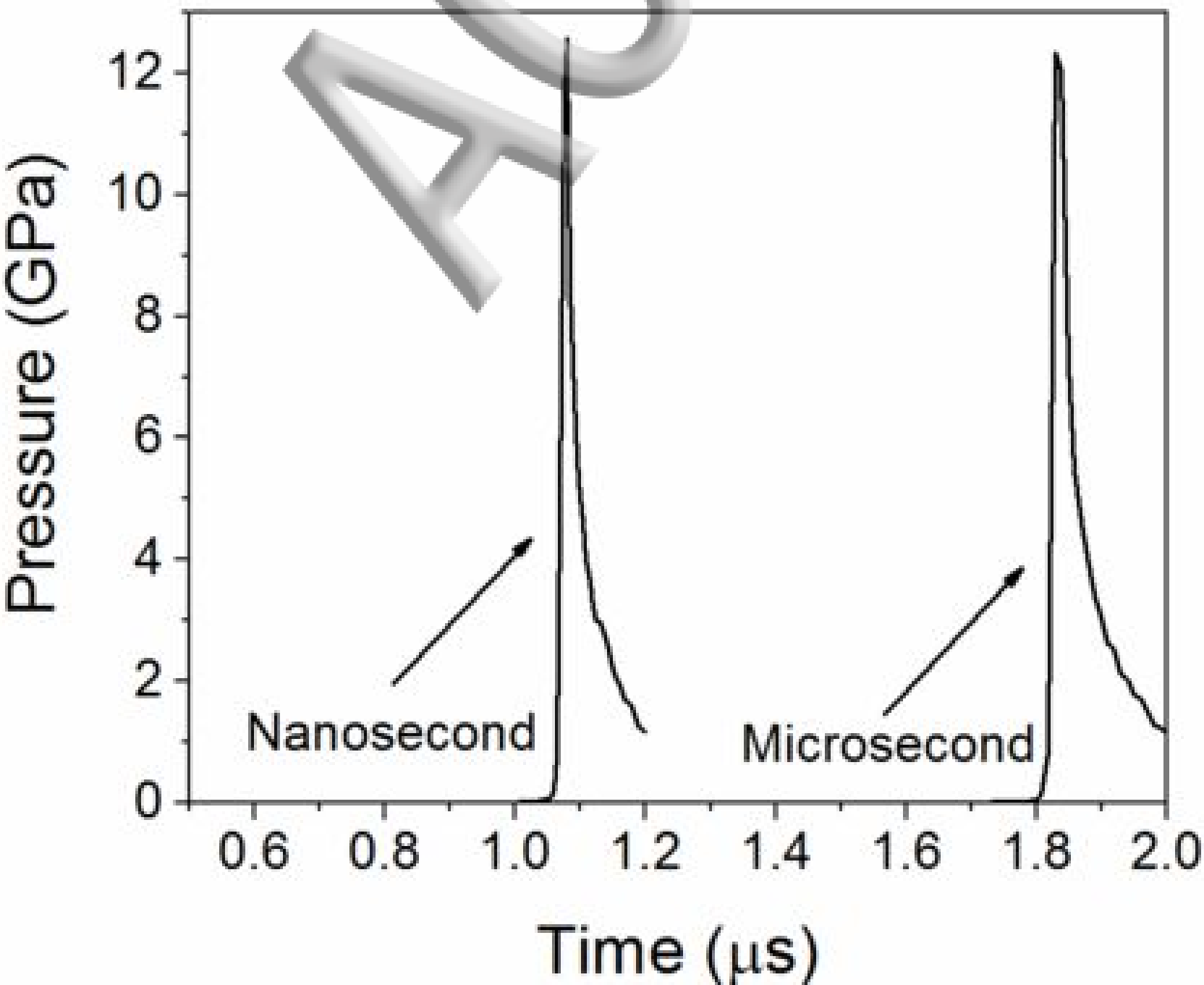
Pressure (GPa)
0
2
4
6
8
10
12
Nanosecond
Microsecond
0.6
0.8
1.0
1.2
1.4
1.6
1.8
2.0
Time (μs)